Proceedings of the 6th International Conference on Gas Hydrates (ICGH 2008),
Vancouver, British Columbia, CANADA, July 6-10, 2008.

GAS HYDRATE FORMATION AND DISSOCIATION FROM WATER-IN-OIL EMULSIONS STUDIED USING PVM AND FBRM PARTICLE SIZE ANALYSIS

John Boxall, David Greaves, James Mulligan, Carolyn Koh and E. Dendy Sloan *
Center for Hydrate Research
Department of Chemical Engineering
Colorado School of Mines
1600 Illinois St, Golden, CO
USA

ABSTRACT

An understanding of the mechanism for hydrate formation from water-in-oil emulsions is integral for progressing from preventing hydrate formation through expensive thermodynamic means to hydrate blockage prevention. This work presents hydrate formation and agglomeration in a stirred system studied using two complementary particle size analysis techniques, a Particle Video Microscope (PVM) and a Focused Beam Reflectance Measurement (FBRM).

The PVM provides qualitative visual information through digital images in the black oil illuminated by a series of lasers. The FBRM provides a quantitative chord length distribution of the particles/droplets in the system. Three sets of experiments were performed using two different Crude oils, Conroe with a very small asphaltene content and poor emulsion stability, and Caratinga with a much higher asphaltene content and emulsion stability. The first experiments looked at ice as an analogy to hydrates, studying the morphology with both the PVM and FBRM. The second experiments looked at the effect of droplet size on hydrate formation and agglomeration, and the third set of experiments studied the dissociation process using a combination of the PVM and *in situ* conductivity measurements to determine the continuous phase.

For hydrate formation, droplet size was found to have a major effect on whether or not agglomeration will occur. During dissociation agglomeration is extremely dramatic due to the creation of surface water on the particles. The dissociation of these agglomerates results in a significant destabilization of the suspension into a water/hydrate phase at the bottom of the cell until dissociation is complete. The dissociation conceptual picture presented illustrates an important implication when operating a flow line with hydrates present; dissociation within the pipeline should be prevented until the hydrates are out of the flow line.

Keywords: hydrate kinetics, hydrate dissociation, agglomeration, cold flow, FBRM, PVM

INTRODUCTION

In the past hydrate prevention methods from water-in-oil emulsions in oil dominated flow line scenarios have been approached with an "avoid at all costs" attitude. This highly conservative approach is largely due to the major difficulties of plug remediation techniques in an oil dominated system as depressurization is often more

* Corresponding author: Phone: +1 303 273 3723 Fax +1 303 273 3730 E-mail: esloan@mines.edu

challenging with the presence of a liquid head. New approaches have started to emerge which change the philosophy toward hydrate management [1] from the often more expensive hydrate prevention. These techniques include the use of anti-agglomerants [2] or cold flow [3]. However, a better understanding of the hydrate formation and agglomeration processes is essential if industry is to move towards hydrate management through plug prevention.

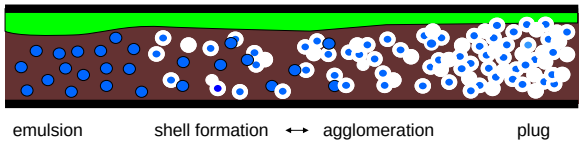

Figure 1. Conceptual picture for hydrate plug formation from a water-in-oil emulsion

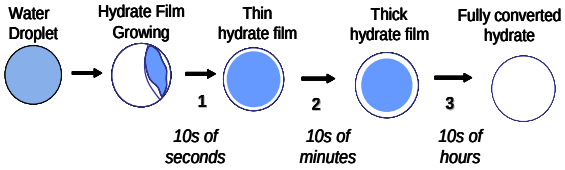

Figure 2. Conceptual picture for the conversion of a water droplet to hydrate

The conceptual pictures for hydrate plugging from a water-in-oil emulsion in Figure 1 (reproduced form Turner, [4]) and for shell formation in Figure 2 (reproduced from Taylor, [5]) suggest six steps are involved in hydrate plug formation from a water-in-oil emulsion in a flow line [6]:

1. The water phase is emulsified within the oil phase with a typical water droplet size of 10-40 µm.
2. Upon hydrate nucleation a hydrate shell grows around the water droplets.
3. The hydrate shell forms a diffusion barrier between the hydrocarbon and water phases.
4. The thick hydrate shell (with occluded water) only fully converts over long times (days).
5. Capillary forces of attraction cause the hydrate-encrusted droplets to agglomerate. These capillary forces are a strong function of temperature; at low temperatures the forces decrease between the particles, as measured by Taylor, [5].
6. As the hydrated particles agglomerate, the effective viscosity increases dramatically, and spikes in the flow line pressure drop occur with time, indicating agglomeration and breakage of hydrate masses. Finally the agglomerates become sufficiently large that flow is stopped, causing flow to be shut in.

The simplified conceptual picture in Figure 1 implies that hydrate agglomeration is often the determining factor in plug formation. If agglomeration can be prevented, for example by using anti-agglomerants or cold flow, one could allow the hydrates to form and flow without obstructing the pipeline. There is evidence that such situations occur in flow lines in Brazil [7], where natural anti-agglomerants exist in oils. The pay off for artificially implementing such techniques is that the high cost of traditional hydrate prevention techniques, such as insulation, can be negated and allow marginal fields to be more economic.

This study focuses on the combined process of hydrate shell formation from small emulsified droplets and agglomeration of the resulting hydrate suspension. The hydrate formation process is compared with the conceptual picture given in Figure 2 and the effect that the formation conditions have on the key steps such as formation of a thick hydrate film and full conversion are discussed. The agglomeration of the hydrate suspension is studied using two particle size analysis techniques, FBRM and PVM. The FBRM technique is used to determine the size distribution of the emulsion before and after hydrate formation to determine the extent to which agglomeration occurs. The PVM technique provides visual evidence during agglomeration of the resulting hydrate suspension.

Experiments were performed in a high pressure autoclave cell pressure rated to 1500 psig with temperature control capable down to -15°C, with greater cooling limited by the choice of cooling fluid. Figure 3 is a schematic representation of the autoclave cell and its various probe attachments. The internal dimensions of the cell are nine inches in height and four inches in diameter; however, a one inch thick false bottom was fashioned for the bottom of the cell and could be easily removed to increase the overall cell volume and adjust the relative position of the particle size analysis (PSA) probes.

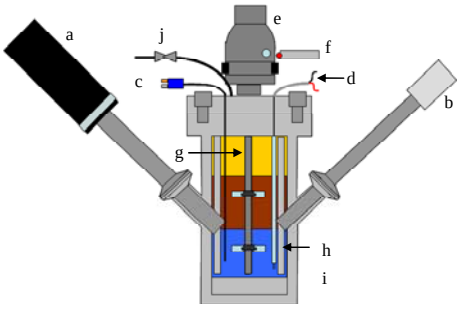

Figure 3. Autoclave cell with attached probes and sensors: (a) PVM probe; (b) FBRM probe; (c) thermocouple; (d) conductivity meter; (e) Magnedrive; (f) tachometer; (g) impeller system; (h) baffles; (i) false bottom; (j) gas inlet.

Two PSA probes were inserted at 45° angles into the cell to maximize flow past the window and facilitate representative measurements of the system. The Focused Beam Reflectance Measurement (FBRM) probe from Mettler-Toledo®, model D600X, has a Class I, 3 MW laser with wavelength 791.8 nm (near infrared) which is transmitted through fiber-optics to the probe tip. A rotating optical lens at the probe tip deflects the laser as shown in Figure 4a. When the probe is inserted into a system of droplets or particles, the laser emitted is reflected if it scans across the surface of a particle, as shown in Figure 4b. The probe measures the reflectance time and determines the chord length by the product of the time and the laser scan speed (scan speed in this work is 4 m/s, but it can range from 2-16 m/s). For more information on the probe and the technique the reader is referred to the FBRM User's Manual [8].

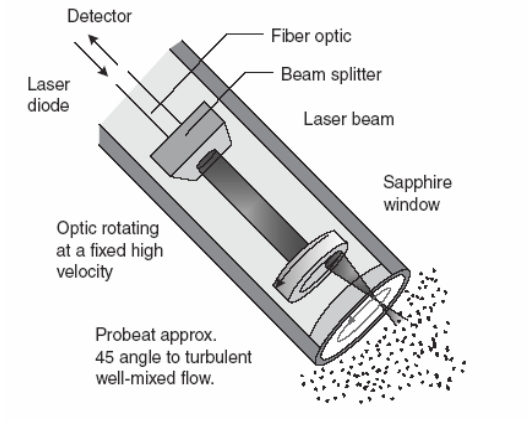

(a)

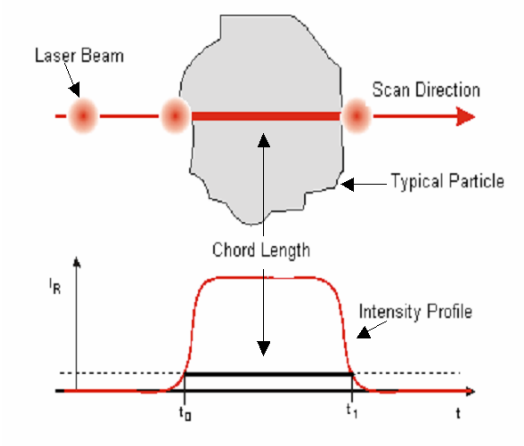

(b)

Figure 4. a) The Focused Beam Reflectance Method (FBRM) probe technique. b) Measurement of a particle chord length using the FBRM technique (illustration from Users Manual).

The Particle Video Microscope (PVM) also from Mettler-Toledo Lasentec® consists of six lasers which illuminate a small area in front of the probe face (Figure 5a). The probe creates digital images of the illuminated area with a field of view of 826 µm x 619 µm. The image provides clear resolution to approximately 20 µm (Figure 5b). For more information on the probe and the technique the reader is referred to the PVM User's Manual [9].

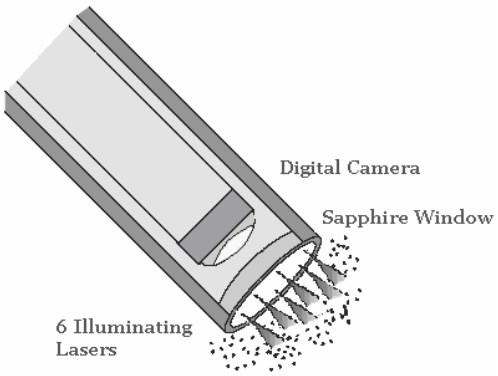

Figure 5. Particle Video Microscope (PVM) probe with six illuminating lasers (850 nm)

To determine the state of the emulsion inside the autoclave cell, an in-house conductivity meter was constructed to withstand high pressures. A Conax-Buffalo® electric feed-through was mounted to the top of the autoclave cell with two wire leads on either end. The internal lead wires were insulated

and ran to the bottom of the cell, with the copper wire exposed 5/16 inches at the end of each wire. The two wire tips were approximately 1/8 inch apart and were located near one of the four baffles, one inch from the bottom of the cell. The external wires were attached in circuit to a data acquisition (DAQ) system, with a nine volt battery providing the voltage for the circuit as shown in Figure 6. Selker et al. [10] used a similar design to construct a conductivity meter but used a resistance bridge to control the voltage rather than a constant voltage.

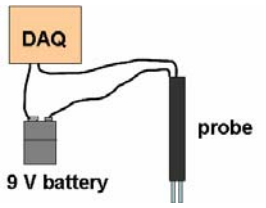

Figure 6. Cartoon of the conductivity meter circuit between the DAQ, the conductivity probe, and the 9V power supply (also shown as Figure 3d).

The autoclave cell shown in Figure 3 was designed to keep the contents well mixed and provide good flow past the face of the PSA probes. However, the shear provided in the autoclave cell is not sufficient to provide the very small droplet sizes of interest for this study. An *ex-situ* emulsion preparation technique was developed using a VirTis Cyclone homogenizer to create the very small droplets, a four-blade turbine impeller to keep the emulsion well mixed, and the FBRM probe to monitor the progress. Figure 7 shows a cartoon of the set-up for the bulk emulsion preparation (BEP) technique. Approximately one liter of water-in-oil emulsion was prepared using this technique with the total mass of the emulsion added to the cell measured.

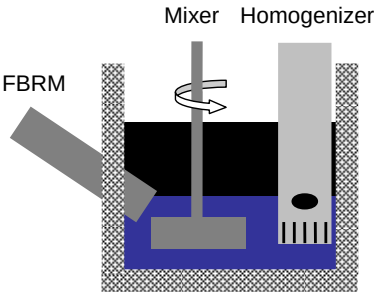

Figure 7. Experimental set-up for the Bulk Emulsion Preparation (BEP) Technique

The two oils used were Conroe crude and Caratinga crude. The Conroe crude is a light crude oil with a specific gravity of 0.84 and a very low asphaltene content (0.31wt%). The Caratinga crude is a much heavier dark crude oil with specific gravity of 0.92 and a much higher asphaltene content (6.2wt%). The gas used was pure methane gas (99.9% purity) or a 75:25 mol% mixture of methane:ethane gas. In all cases the water used was distilled water with no salts added.

RESULTS

Ice as an Analogy to Hydrate

The Particle Video Microscope probe gives visual images of the solid suspensions in the crude oil which allows the morphology of the crystals to be studied. In Figure 8 the morphology of methane hydrate (a) and ice (b) are compared. Both hydrate and ice were formed from an emulsion with 30% water cut in the Conroe crude oil. The major difference between the two solid suspensions is that the agglomerates formed with hydrates have a much more amorphous structure whereas the ice agglomerates appear to be made up of aggregated spherical ice particles.

The difference in morphology is also observed with the FBRM measurements, given in Figure 9. For each experiment the FBRM chord length distributions are compared before hydrate/ice nucleation, during formation, then after dissociation/melting. The FBRM distribution for the hydrate formation (Figure 9a) changes dramatically during formation with larger chord sizes being measured and retains larger size measurements after dissociation. In contrast the FBRM distribution for the ice formation (Figure 9a) remains relatively unchanged after freezing and also after melting of the ice back into a water-in-oil emulsion. This suggests that the FBRM measurements of the ice suspensions are of each individual ice particle in the agglomerate and not the full agglomerate for the coarse ice clusters.

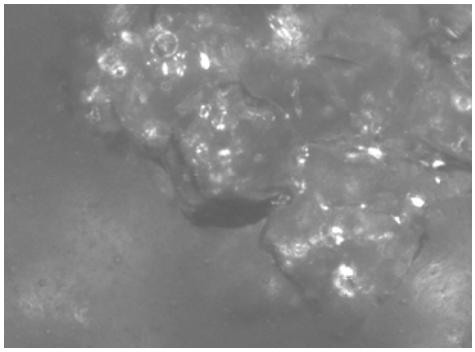

(a)

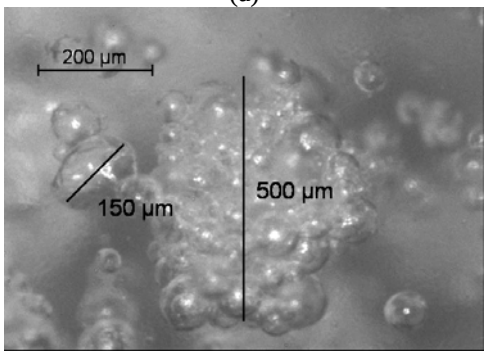

(b)

Figure 8. PVM images of a methane hydrate suspension (a) and an ice suspension (b) from Conroe crude oil with 30% water cut

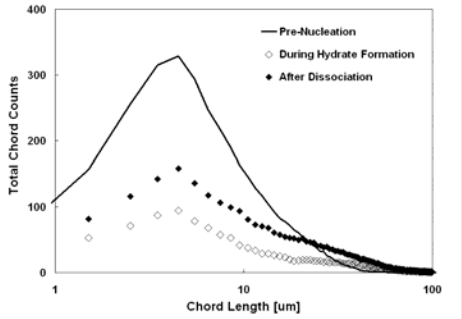

(a)

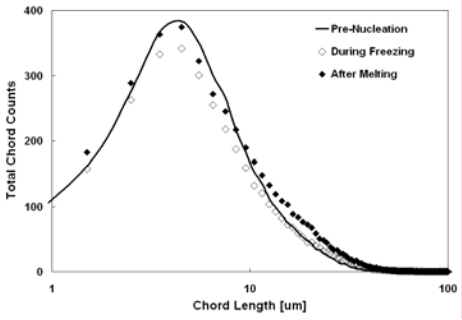

(b)

Figure 9. FBRM measurements of a methane hydrate suspension (a) and an ice suspension (b) from Conroe crude oil with 30% water cut

Hydrate Formation Experiments

For the hydrate formation experiments the effect the droplet size has on both the formation and agglomeration was studied. Three size distributions each with a 30% water cut were studied with the distributions measured by examining a drop of the water-in-oil emulsion on a glass slide and placed under the microscope. The image analysis software, ImageJ, was used to measure the droplet diameter size distributions for each sample.

The first distribution was an extremely fine emulsion created by homogenizing at 16,000 rpm. The resulting size distribution was less than 5µm (Figure 10a) with most droplets too small to be measured. The second was homogenized at 8000 rpm and the droplet diameter distribution was measured between 5-15µm (Figure 10b). The third distribution was not homogenized but just mixed at 600 rpm until the FBRM distribution was stable. This resulted in droplet diameters measured between 20-150µm (Figure 10c).

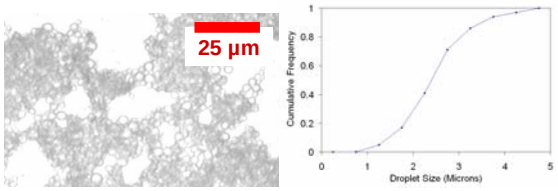

(a) Homogenized @ 16.000 rpm

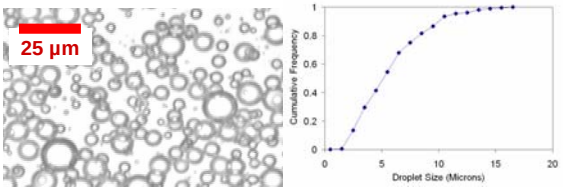

(b) Homogenized @ 8000 rpm

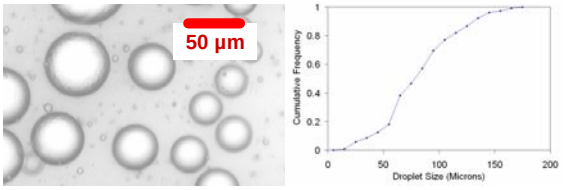

(c) Mixed @ 600 rpm

Figure 10. Microscope images and droplet diameter distributions for the three emulsions created using the BEP technique

The three hydrate formation/dissociation experiments were performed with the Caratinga oil using the following procedure:

1. Form emulsion using Bulk Emulsion Preparation (BEP) technique
2. Pour emulsion into autoclave cell noting the mass of emulsion added
3. Pressurize cell to 950psi at 20°C until oil is saturated
   - Methane gas used (sI hydrates)
   - Gas introduced at bottom of cell to eliminate mass transfer resistance from gas to oil
4. Cool cell to 1°C under constant pressure
   - Equilibrium Temp = 9.1°C (CSMGem[6]) or 8°C sub-cooling
5. Form hydrate until conversion stops
   - Conversions calculated using a ratio of CH_4 to H_20 in the hydrate of 6.1 to 1 (CSMGem)
6. Dissociate using constant pressure

Figure 10 shows the hydrate formation result for the emulsions prepared by homogenizing at 16,000 rpm and at 8000 rpm. The hydrate formation rates were similar for the two smallest size distributions and the overall conversion of water to hydrate was the same between the two runs. The total water conversion for the two runs may represent the maximum conversion for the apparatus and/or conditions used.

Figure 11 compares the hydrate formation results for the large droplets of the un-homogenized emulsion (mixed at 600 rpm) and the 8000 rpm homogenized case. The larger droplets of the un-homogenized case results in much slower conversion of water to hydrate. This slowed formation rate is most likely due to mass transfer limitations from diffusion through the thick hydrate shell.

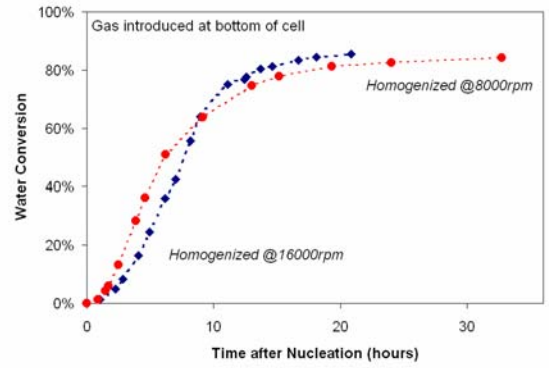

Figure 10. Hydrate formation for the emulsions created at 16,000rpm and 8000 rpm

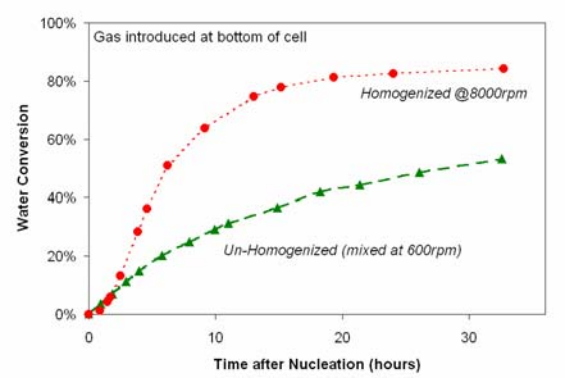

Figure 11. Hydrate formation for the emulsions created at 8000rpm and 600 rpm

Figures 12 and 13 show the FBRM distribution measurements for the 8000 rpm homogenized experiment and the 600 rpm un-homogenized experiment. The FBRM distributions shown are before and after hydrate formation/dissociation, or after step 3 and step 6 of the outlined procedure and are both measured when the system is at 20°C and 950 psi.

Figure 12 shows that there is very little change in the FBRM distribution measured for the small (<15µm) droplets upon formation/dissociation but there is a significant change in the FBRM distribution for the larger (20-150µm) droplets (Figure 13). The total shear in the system is less than the original applied during the emulsion preparation procedure and certainly less than what is required to re-homogenize the emulsion. This result shows that little-to-no agglomeration of the hydrate particles is observed for the small droplet emulsion during hydrate formation/dissociation resulting in the same FBRM distribution. In-contrast, significant agglomeration is inferred during hydrate formation/dissociation for the large droplet case due to the significant shift of the FBRM distribution to the right suggesting much larger droplets are now present.

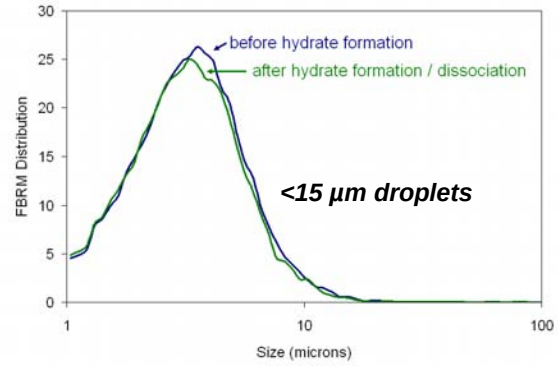

Figure 12. FBRM distributions of the emulsion prepared at 8000 rpm, before and after hydrate formation/dissociation

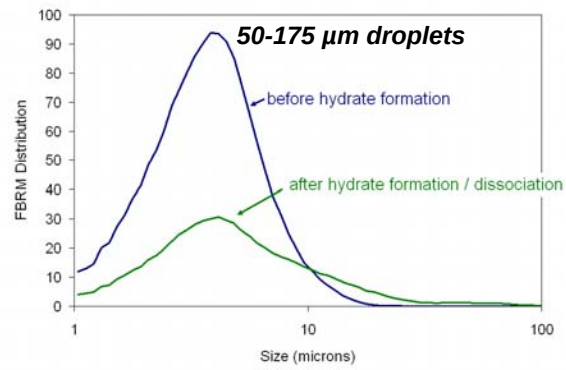

Figure 13. FBRM distributions of the emulsion prepared at 600 rpm, before and after hydrate formation/dissociation

Dissociation of the Hydrate Suspension

Conductivity measurements combined with visual PVM images have been used to illustrate the effect dissociation has on the hydrate suspension and the resulting water-in-oil emulsion. Hydrate formation and dissociation experiments were performed in Conroe crude with a 30% water cut and constant (75% methane, 25% ethane) gas volume. Figure 14 shows a plot of cell pressure (which shows the extent of hydrate dissociation) and the relative conductivity at the bottom of the cell which indicates the state of the emulsion (a high conductivity indicates water as the continuous phase). The time labels (a-h) correspond to PVM images shown in Figure 15. These images show what is happening during hydrate dissociation and correspond nicely with the conductivity changes shown in Figure 14.

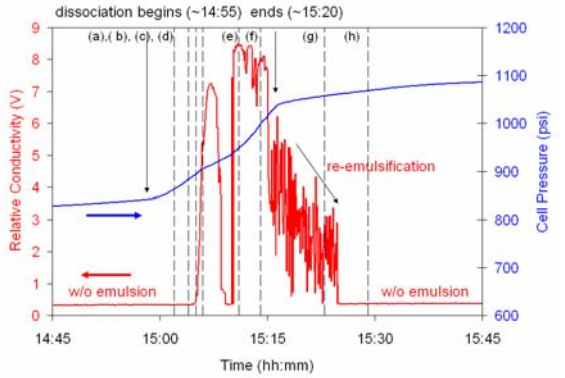

Figure 14. Hydrate dissociation for Conroe crude oil with 30% water cut

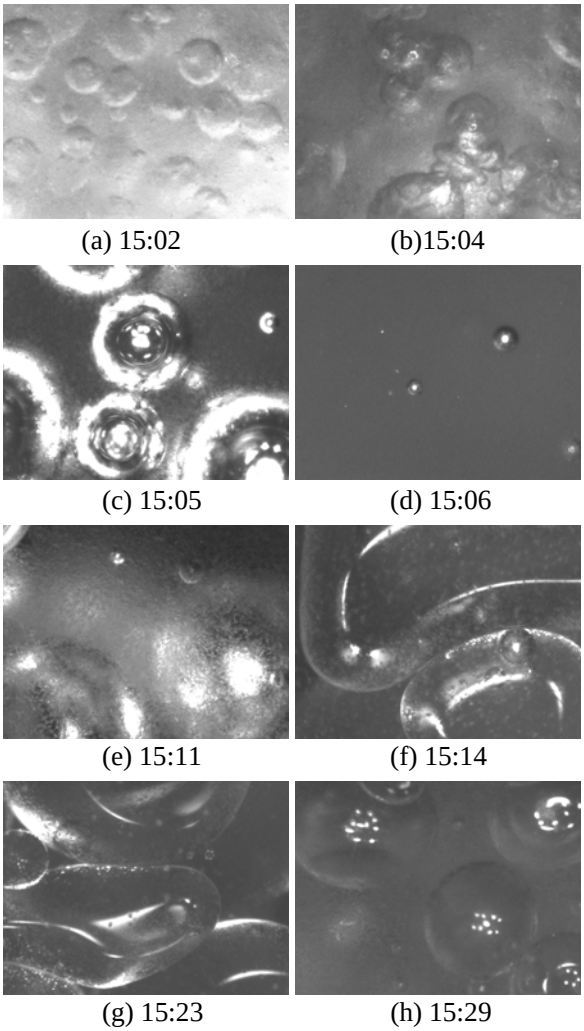

Figure 15. PVM images during dissociation for Conroe crude oil with 30% water cut.

The Conroe crude oil represents a crude oil with poor emulsion stability and has relatively low asphaltene content (0.31wt%). The experiment shown in Figures 14 and 15 were repeated using a different crude oil that has a much stronger emulsion stability and much higher asphaltene content (6.2wt%), Caratinga crude oil. Lachance [11] studied the emulsion stability of both of these crude oils. The dissociation experiment for the more stable Caratinga oil and corresponding PVM images is given in Figure 16. A very similar result is observed were the conductivity spikes during the dissociation of the hydrate indicating that the emulsion destabilizes with water as the continuous phase at the bottom of the cell. Once the hydrate has fully dissociated the emulsion is then quickly re-emulsified and the conductivity indicates the oil as the continuous phase.

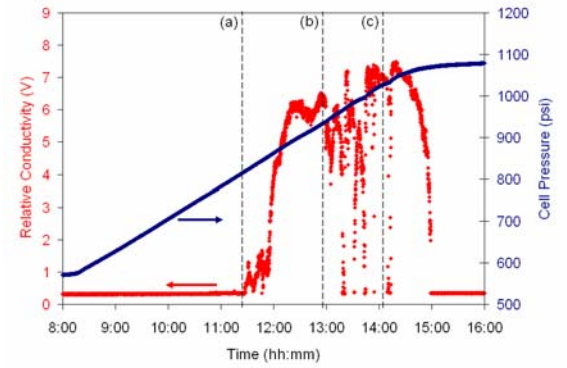

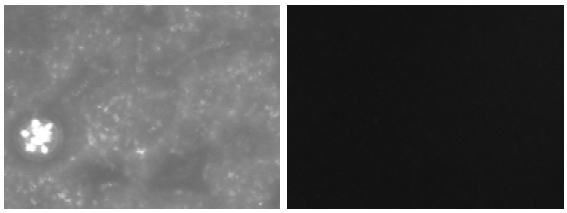

(a) 15:02 (b)15:04

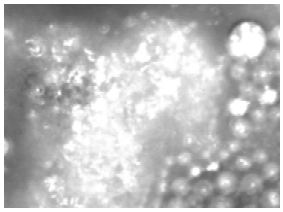

(c) 15:05

Figure 16. Hydrate dissociation for Caratinga crude oil with 30% water cut with corresponding PVM images.

The experiment shown in Figure 16 was for the un-homogenized case with larger (20-150µm) droplets. An equivalent experiment was performed where the emulsion was homogenized at 8000 rpm (producing 5-15µm droplets). No destabilization of the hydrate suspension through increased conductivity measurements was observed during dissociation of the hydrates suggesting that this effect is dependant on the hydrate particle size. Future work will look at the threshold particle size.

Figure 17 illustrates a conceptual picture for the hydrate dissociation process happening in the FBRM/PVM apparatus, as shown by the PVM images and the conductivity results.

(i) initially the system starts as a hydrate suspension (15a)
(ii) as the hydrate starts to dissociate the particles tend to aggregate more (15b)
(iii) gas is released and the large aggregates settle (with continuous mixing) as can be seen in the conductivity increase and images (15c), (15d) and (15e)
(iv) with hydrates still present the system does not emulsify the water/hydrate very well, very large droplets containing hydrate flakes can be seen (15f), (15g)
(v) once all hydrate has been dissociated the system, under continuous shear, once again is emulsified (15h)

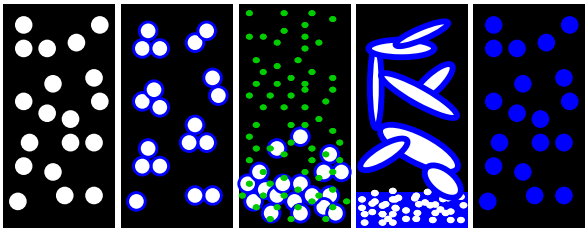

(i) (ii) (iii) (iv) (v)

Figure 17. Cartoon illustrating the conceptual picture for dissociation of a hydrate suspension.

CONCLUSIONS

The morphology of ice appears significantly different to that for hydrates for formation from a water-in-oil emulsion. Ice keeps its spherical shape and aggregates into clusters of solid spheres, whereas hydrates will form more amorphous agglomerates. This result was corroborated by the FBRM distribution for the two systems. For the ice the FBRM distribution was very similar before ice formation, with ice particles, and after ice

dissociation. The FBRM distribution for the hydrate system changed dramatically during formation, measuring larger sizes.

Methane hydrate formation/dissociation experiments were performed using water-in-oil emulsions with three different size distributions (<5μm, <15μm, 20-150μm). The two smallest droplet size cases formed quickly until completion with about 85% conversion of the overall water. The largest droplets did not form to completion (after 32 hours) with further formation most likely limited by diffusion through the thick hydrate shell. FBRM distributions before and after hydrate formation showed that significant agglomeration occurred for the larger droplet sizes during the formation/dissociation of the hydrates but showed little evidence of any agglomeration of the smaller (<15μm) droplets.

A conceptual picture for hydrate dissociation is presented showing the destabilizing nature of hydrate on water-in-oil emulsions. The particle size has an important role; however, hydrate suspensions formed from very small droplet sizes (<15μm hydrate particles) did not show the same destabilizing behavior.

ACKNOWLEDGEMENTS

The authors wish to acknowledge the financial support received from the CSM hydrate consortium of energy companies: BP, Champion, Chevron, ConocoPhillips, ExxonMobil, Halliburton, Petrobras, Schlumberger, Shell, and StatoilHydro.

REFERENCES

[1]Sloan, E.D., *Seven Industrial Hydrate Flow Assurance Lessons From 1993-2003*, Proceedings of the Fifth International Conference on Gas Hydrates, June 12-16, 2005. Trondheim, Norway

[2]Mehta, A.P., Hebert, P.B., Cadena, E.R., Weatherman, J.P., *Fulfilling the Promise of Low-Dosage Hydrate Inhibitors: Journey From Academic Curiosity to Successful Field Implementation*, SPE Production & Facilities, 73, 2003

[3]Wolden, M., Lund, A., Oza, N., Makogaon, T., Argo, C.B., Larsen, R., *Cold Flow Black Oil Slurry Transport of Suspended Hydrate and Wax Solids*. Proceedings of the Fifth International Conference on Gas Hydrates, June 12-16, 2005. Trondheim, Norway

[4]Turner, D., *Clathrate hydrate formation in water-in-oil dispersions*, Ph.D. thesis, Colorado School of Mines, Golden, CO. 2005

[5]Taylor, C. J. *Adhesion Force between Hydrate Particles and Macroscopic Investigation of Hydrate Film Growth at the Hydrocarbon/Water Interface*, Master thesis, Colorado School of Mines, Golden, CO, 2006

[6]Sloan, E.D., and Koh, C.A., *Clathrate Hydrates of Natural Gases, 3rd Ed.* CRC Press, Taylor and Francis Group, LLC, 2008

[7]Palermo, T., A. Mussumeci, et al. *Could Hydrate Plugging Be Avoided Because of Surfactant Properties of the Crude and Appropriate Flow Conditions?* Offshore Technology Conference OTC 16681, 2004

[8]Mettler-Toledo Lasentec® Product Group, 2001. *Lasentec® D600 Hardware Manual*. Mettler-Toledo AutoChem, Inc., Redmond, WA.

[9]Mettler-Toledo Lasentec® Product Group, 2002. *Lasentec® PVM User Manual*. Mettler-Toledo AutoChem, Inc., Redmond, WA.

[10] Selker, A. H. and J. C.A. Sleicher, *Factors Affecting which Phase will Disperse when Immiscible Liquids are Stirred Together*. The Canadian Journal of Chemical Engineering 43: 295-301, 2006.

[11] Lachance, J., *Investigation of Gas Hydrates using Differential Scanning Calorimetery with Water-in-oil Emulsions*, Master thesis, Colorado School of Mines, Golden, CO, 2008